MOLECULAR AND CELLULAR BIOLOGY, Mar. 2003, p. 1817–1831 Vol. 23, No. 5
0270-7306/03/$08.00+0 DOI: 10.1128/MCB.23.5.1817–1831.2003


# A Mutant Receptor Tyrosine Phosphatase, CD148, Causes Defects in Vascular Development

Takamune Takahashi,[1]* Keiko Takahashi,[1] Patricia L. St. John,[2] Paul A. Fleming,[3] Takuya Tomemori,[4] Toshio Watanabe,[5] Dale R. Abrahamson,[2] Christopher J. Drake,[3] Takuji Shirasawa,[4] and Thomas O. Daniel[6]

*Nephrology Division and Center for Vascular Biology, Vanderbilt University Medical Center, Nashville, Tennessee 37232[1]; Department of Anatomy and Cell Biology, University of Kansas Medical Center, Kansas City, Kansas 66160-0003[2]; Department of Cell Biology, Medical University of South Carolina, Charleston, South Carolina 29425[3]; Immunex Corporation, Seattle, Washington 98101[6]; and Department of Molecular Genetics, Tokyo Metropolitan Institute of Gerontology, Tokyo 173,[4] and Institute of Development, Aging, and Cancer, Tohoku University, Sendai 980,[5] Japan*

Received 9 July 2002/Returned for modification 10 September 2002/Accepted 11 December 2002

**Vascularization defects in genetic recombinant mice have defined critical roles for a number of specific receptor tyrosine kinases. Here we evaluated whether an endothelium-expressed receptor tyrosine phosphatase, CD148 (DEP-1/PTPη), participates in developmental vascularization. A mutant allele, CD148$^{\Delta CyGFP}$, was constructed to eliminate CD148 phosphatase activity by in-frame replacement of cytoplasmic sequences with enhanced green fluorescent protein sequences. Homozygous mutant mice died at midgestation, before embryonic day 11.5 (E11.5), with vascularization failure marked by growth retardation and disorganized vascular structures. Structural abnormalities were observed as early as E8.25 in the yolk sac, prior to the appearance of intraembryonic defects. Homozygous mutant mice displayed enlarged vessels comprised of endothelial cells expressing markers of early differentiation, including VEGFR2 (Flk1), Tal1/SCL, CD31, ephrin-B2, and Tie2, with notable lack of endoglin expression. Increased endothelial cell numbers and mitotic activity indices were demonstrated. At E9.5, homozygous mutant embryos showed homogeneously enlarged primitive vessels defective in vascular remodeling and branching, with impaired pericyte investment adjacent to endothelial structures, in similarity to endoglin-deficient embryos. Developing cardiac tissues showed expanded endocardial projections accompanied by defective endocardial cushion formation. These findings implicate a member of the receptor tyrosine phosphatase family, CD148, in developmental vascular organization and provide evidence that it regulates endothelial proliferation and endothelium-pericyte interactions.**

A number of cell surface receptors coupled with activating ligands play central roles in the coordination of embryonic vascular development and postnatal neovascularization (11, 37). Prominent among these coordinators of development and neovascularization are vascular endothelial growth factor (VEGF) and its receptors VEGFR1 and -2 (Flt-1 and KDR/Flk1); ephrin-B2 and its receptor EphB4; angiopoietins 1 and 2 and the Tie2 receptor; platelet-derived growth factor (PDGF)-B and PDGFβ receptor; receptors for the transforming growth factor β (TGFβ) superfamily (TGFβ type II receptor, activin-receptor-like kinase 1 [Alk1], and endoglin) (32, 34, 35); and Jagged1 and Notch1 and -4 (28, 51).

Coordinated assembly of vascular elements requires regulated signaling to control at least three functional components of the process. These include (i) differentiation and expansion of endothelial progenitors, (ii) assembly and differential growth of interconnecting vascular networks, and (iii) progressive investment and maturation of vessels with supportive structures, including either pericytes (PCs) or vascular smooth muscle cells (vSMCs). The VEGFs and their receptors are required for endothelial differentiation and primary capillary plexus formation in vasculogenesis (18). Both the ephrin-B2 transmembrane counterreceptor and EphB4 receptor are essential for interconnection and maturation of primary arterial and venous limb vascular plexus structures (1). PDGF-B and PDGFβ receptors participate in PC differentiation and recruitment (33). The angiopoietins and Tie2 receptor mediate vascular remodeling and maturation by regulating endothelial sprouting and endothelium-PC interactions (23).

Although coupled and counterbalancing roles for receptor tyrosine kinases and phosphatases have been well defined in neural targeting and differentation systems (13, 48), functional roles for endothelial receptor tyrosine phosphatases have yet to be defined in vascular development. Within the very large family of receptor protein tyrosine phosphatases, RPTPμ, HPTPβ/VE-PTP, and CD148/DEP-1/PTPη are known to be expressed on vascular endothelial cells. RPTPμ mediates homophilic intercellular binding, associates with cadherin-catenin complexes, and appears to participate in endothelial intercellular adhesion (6, 9). VE-PTP/HPTPβ is widely expressed in endothelium throughout mouse development and associates with Tie2 receptor, reducing the phosphotyrosine content of the receptor (17). CD148/DEP-1/PTPη is expressed in a range of hematopoietically derived cell lineages (12) as well as in the vascular endothelial cells of the arterial and capillary vessels of a number of organs (7, 45).

CD148 has been implicated in the arrest of cell growth and

* Corresponding author. Mailing address: Department of Medicine, Nephrology Division, Vanderbilt University Medical Center, S-3223, MCN, Nashville, TN 37232-2372. Phone: (615) 322-4794. Fax: (615) 343-7156. E-mail: takamune.takahashi@mcmail.vanderbilt.edu.

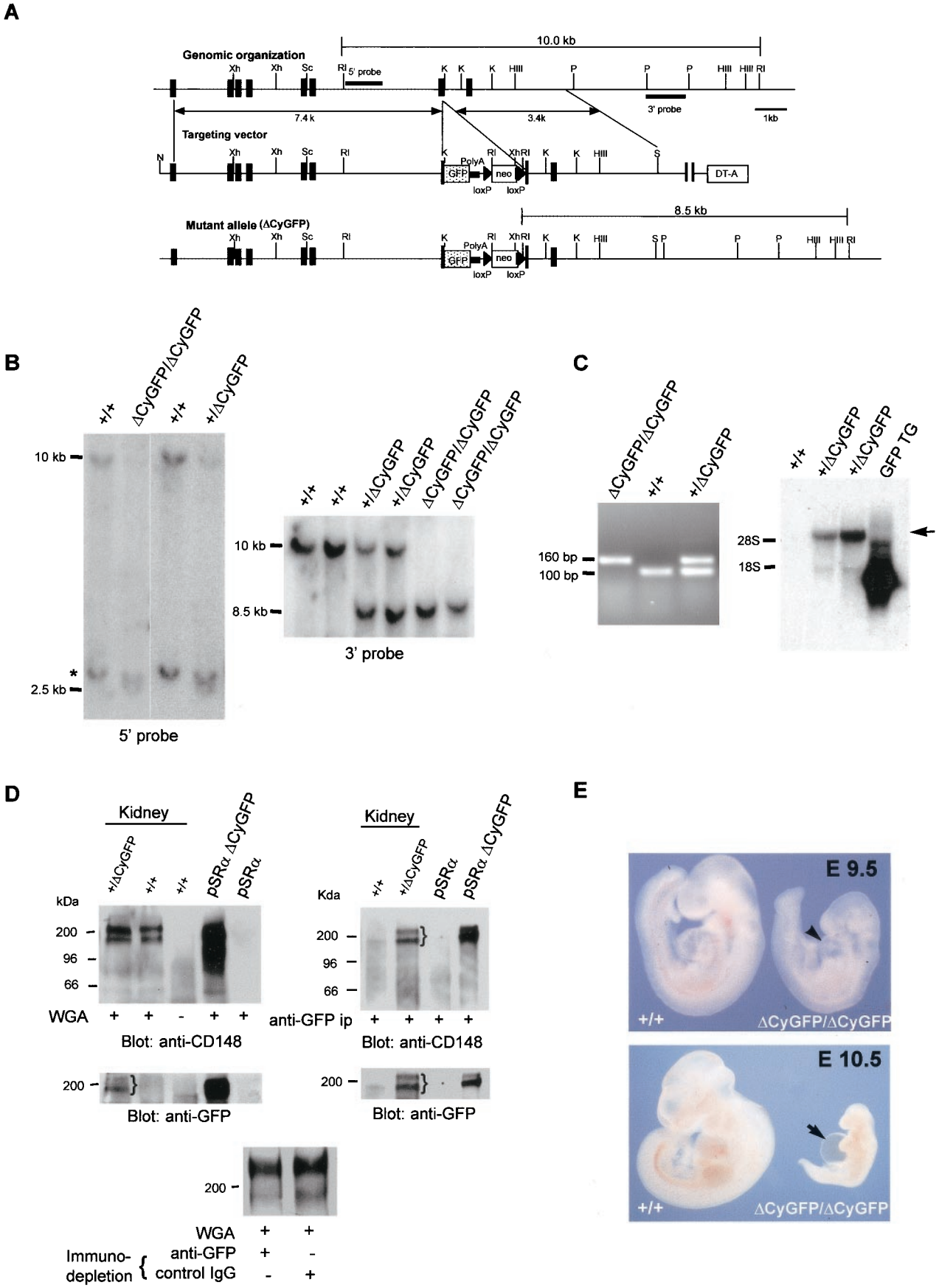
A
Genomic organization
10.0 kb
5' probe
3' probe
7.4 k
3.4k
1kb
Targeting vector
PolyA
GFP
neo
loxP
DT-A
Mutant allele (ΔCyGFP)
8.5 kb
B
+/+
ΔCyGFP/ΔCyGFP
+/ΔCyGFP
10 kb
2.5 kb
5' probe
8.5 kb
3' probe
C
160 bp
100 bp
28S
18S
GFP TG
D
Kidney
pSRα ΔCyGFP
pSRα
kDa
200
96
66
WGA
anti-GFP ip
Blot: anti-CD148
Blot: anti-GFP
Immuno-depletion
anti-GFP
control IgG
E
E 9.5
E 10.5

activation in a number of settings, and several of its features are distinct from those of other endothelium-expressed receptor tyrosine phosphatases. Initially identified in a HeLa cDNA library by homology cloning, CD148/DEP-1 was shown to increase in abundance in densely cultured lung fibroblasts (thus the name "density-enhanced phosphatase") (36). As a member of a small subfamily of receptor tyrosine phosphatases, CD148 is a type I membrane protein comprised of at least eight extracellular fibronectin type III motifs, a membrane-spanning region, and a single intracellular phosphatase domain (36). In addition to its expression in hematopoietic and endothelial lineages, CD148 is expressed in duct epithelia of thyroid and mammary tissues (27, 53). Reduction of CD148 expression correlates with a malignant phenotype in thyroid tumors and breast cancer-derived cell lines (27, 53). Its expression is induced during differentiation of breast tumor cells and erythroleukemia cells (27, 29). Induced overexpression of CD148 inhibits tumor cell growth by suppressing mitogen-activated protein kinase activation and increasing p27 stability (47). CD148 overexpression inhibits c-*fos* and cyclin A promoter activity in endothelial cells (43). Inducible expression of CD148 inhibits coupling of T-cell activation to phospholipase-γ1 dephosphorylation and LAT reduction (2). More recently, Ptprj (CD148) has been shown to be a candidate for the mouse colon-cancer susceptibility locus, Scc1, and has been found to be frequently mutated in human cancers (40). In the aggregate, these findings argue that CD148 imposes regulation of cell growth and differentiation.

Our finding that CD148 is expressed at high levels in endothelia, including developing renal vascular endothelia, led us to address whether its function is important in developmental vascularization. Here we report the generation of homologous recombinant mice expressing a mutant CD148 ($CD148^{\Delta CyGFP}$) from which cytoplasmic phosphatase sequences have been removed and substituted in frame by sequences encoding enhanced green fluorescent protein (EGFP) to create a CD148/GFP fusion protein. Developmental consequences of this knock-in mutation in homozygous mutant embryos are severe, with death at 10.5 days of gestation, accompanied by failure of developmental vascularization and associated growth retardation.

## MATERIALS AND METHODS

**Targeted disruption of the mouse CD148 gene.** A 12-kb genomic fragment encoding the catalytic domain of PTPβ-2/Byp-1 (a murine homologue of human CD148) (29, 30) was isolated from a 129/Sv genomic library (Stratagene). An EGFP-coding gene (Clontech) was fused in frame to the murine CD148 gene at the *Kpn*I site. This EGFP insertion results in a catalytically inactive CD148-GFP fusion gene ($CD148^{\Delta CyGFP}$), substituting GFP for the C-terminal 117 amino acid residues containing essential cysteine and the surrounding core motif. An additional *Eco*RI site was introduced into the mutant allele to distinguish wild-type (10.0 kb) from targeted (2.5 kb with a 5′ probe and 8.5 kb with a 3′ probe) alleles when probed with a 5′ probe, a 0.5-kb *Eco*RI-*Afl*II fragment, and a 3′ external probe, a 0.9-kb *Pst*I-*Pst*I genomic fragment. The pMCDT-A (A+T/pau) vector (52) and a *loxP*-flanked *neo* cassette (from T. Yagi, National Institute for Physiological Sciences, Okazaki, Japan) were used to construct the targeting vector. TL1 embryonic stem (ES) cells (54) were electroporated with the linearized targeting vector and selected with G418, and the genotype was analyzed by Southern blotting. Two correctly targeted clones (out of 192 clones) were injected into blastocysts of C57BL/6J mice. Germ line transmission of the two independently targeted ES clones was confirmed by Southern blotting. Subsequent genotyping was performed using an LA-PCR kit (Takara). Primers for intronic fragments (forward, 5′-GGCCAGCTTGATTTCACTCACCG-3′; reverse, 5′-GAGTCCTGCCACTATCTGGCATG-3′) were used.

**Reverse transcription-PCR and Northern blot analysis.** Using RNA STAT-60 (Tel-Test, Inc.), total RNA was extracted from yolk sac tissues. Single-stranded cDNA synthesis and PCR amplification were carried out using Ready-To-Go reverse transcription-PCR (RT-PCR) beads (Amersham Pharmacia Biotech) according to the manufacturer's instructions. The 5′ primer for the upstream sequence of the targeted site (5′-ACCACGGTGTTCCTGACA-3′) and the 3′ primers for the wild-type catalytic domain (5′-GCAATGCACCAGAATTGG-3′) and EGFP gene (5′-TTGTGGCCGTTTACGTCG-3′) were used. The PCR products were separated by 2% agarose gel and visualized with ethidium bromide. Using an RNeasy kit (Qiagen), total RNA was extracted from adult kidneys for Northern blot analysis. Northern hybridization was carried out using a 0.7-kb EGFP cDNA fragment as a probe.

**Wheat germ agglutinin affinity, immunoprecipitation, and Western blotting.** Adult kidneys were removed from 6-week-old wild-type and heterozygous mice. A 10% (wet wt/vol) tissue lysate was prepared by homogenizing the tissue in lysis buffer (50 mM Tris [pH 7.5], 150 mM NaCl, 1% Triton X-100, 0.5% deoxycholate, 1 mM EDTA) containing protease inhibitor cocktail (Complete Mini; Roche Applied Science). After 30 min on ice, the homogenates were clarified twice by centrifugation at 15,000 × *g* for 30 min. The CD148 proteins were recovered by incubating 5 mg of tissue lysates with wheat germ agarose beads (Sigma) overnight at 4°C. For anti-GFP immunoprecipitation, the tissue lysate

FIG. 1. Targeted mutation of the mouse CD148 gene. (A) Schematic diagram (from top to bottom) of the wild-type CD148 allele encoding the cytoplasmic domain, the targeting vector, and the recombinant mutant allele, $CD148^{\Delta CyGFP}$. Exons are indicated by vertical black rectangles. The phosphatase domain was disrupted by an in-frame insertion of the enhanced GFP coding sequence, as described in Materials and Methods. The *loxP* (black triangle)-flanked neomycin cassette (neo) permitted positive selection and subsequent excision by Cre recombinase, while the diphtheria toxin A cassette, DT-A, negatively selected nonhomologous recombinants. Xh, *Xho*I; RI, *Eco*RI; K, *Kpn*I; P, *Pst*I; Sc, *Sca*I; HIII, *Hin*dIII; S, *Sal*I. (B) Southern blot analysis of E9.5 embryos from $CD148^{+/\Delta CyGFP}$ heterozygote intercrosses. Using the 5′ (10.0 kb and 2.5 kb) and 3′ (10.0 kb and 8.5 kb) probes as indicated in panel A, *Eco*RI restriction fragments were used to distinguish wild-type from mutant alleles. The asterisk indicates the presence of a pseudogene. (C) RT-PCR analysis of E9.5 yolk sac mRNA. Amplified products, determined using the primer set described in Materials and Methods, were 104 bp (wild type) and 159 bp (mutant), as predicted. (Right panel) Northern blot analysis of total RNA from adult kidneys. Total RNA was isolated, transferred, and hybridized with GFP cDNA probe (see Materials and Methods), using RNA from a GFP transgenic mouse (GFP TG) (20) as a positive control. The predicted 5.2-kb $CD148^{\Delta CyGFP}$ transcript (arrow) was detected in heterozygous mice. (D) Western blot analysis of adult mouse kidneys. Expressed CD148 forms were recovered from adult kidney extracts by a lectin (wheat germ agglutinin [WGA] from *Triticum vulgaris*) affinity step (left panel) or by GFP antibodies (right panel) and detected on immunoblots with an ectodomain interactive anti-CD148 or anti-GFP antibody. A doublet (brace) expressed from the mutant allele at approximately 200 kDa that demonstrates similar glycosylation heterogeneity to that of the native protein is recovered by lectin and by anti-GFP at a mass similar to that of the wild-type protein. The CHO cell lysates transfected with empty vector (pSRα) and $CD148^{\Delta CyGFP}$ expression plasmid (pSRα ΔCyGFP) were used as controls. Immunodepletion experiments using anti-GFP showed an approximately 30% reduction of CD148 compared with those using a control (bottom panel). (E) Photomicrographs of wild-type and $CD148^{\Delta CyGFP}$ homozygous embryos at E9.5 to 10.5. Homozygous mutant embryo at E9.5 shows reduced size, edema, and distended pericardium (arrowhead). At E10.5, severe growth retardation and prominent extension of pericardial sac (arrow) were noted.

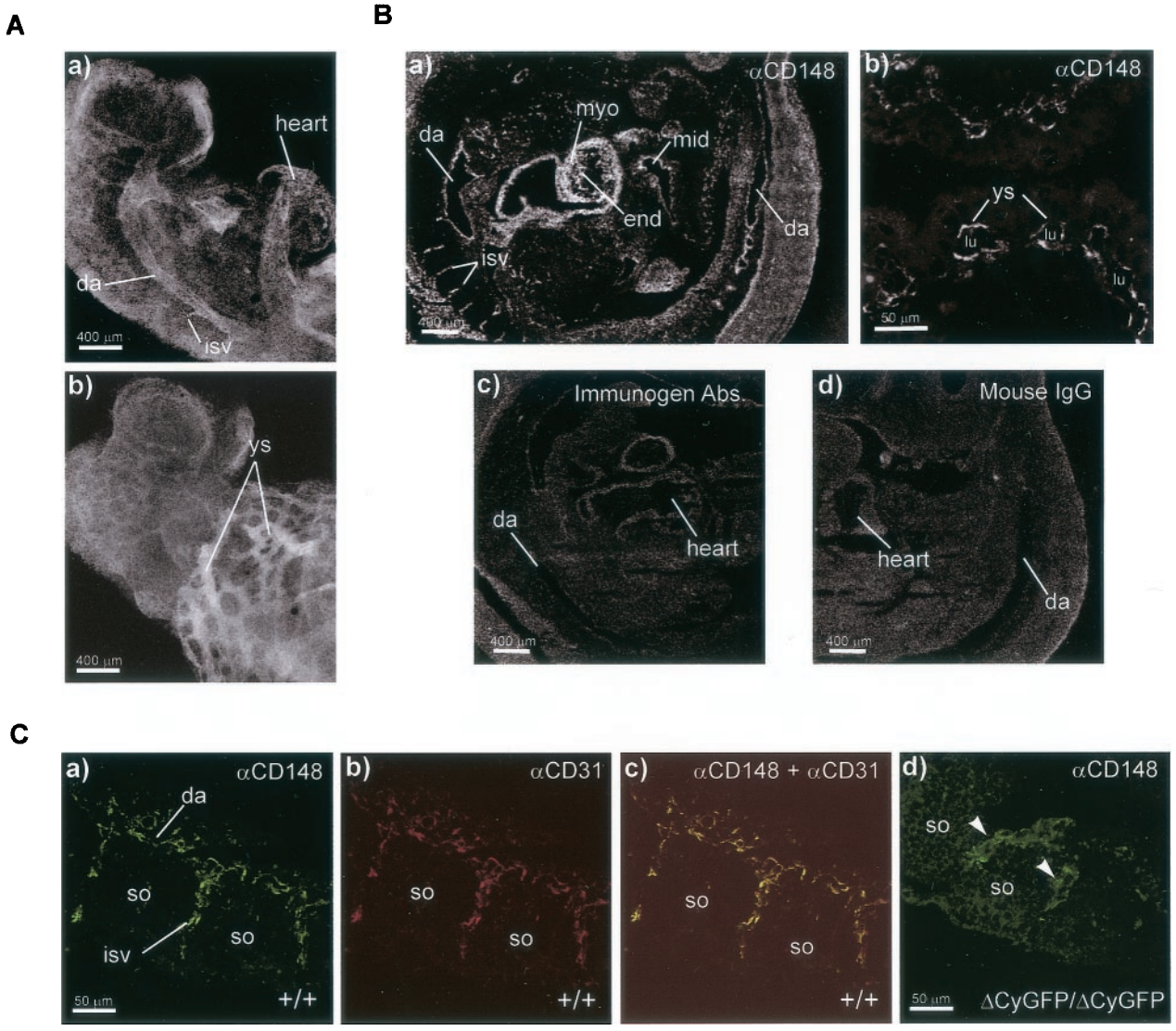


FIG. 2. CD148 immunolocalization in midgestation embryos. (A) Whole-mount CD148 immunostaining of a wild-type embryo at E9.0. Monoclonal anti-CD148-labeled embryonic vasculature, including dorsal aorta (da), heart, intersomitic vessels (isv), and yolk sac vessels (ys), is shown. Panel a and panel b show the cranial half of the embryo. (B) Immunofluorescence staining of E10.0 wild-type embryo frozen sections. A sagittal section of the embryo (a) and a yolk sac cross-section (b) localize CD148 expression in the endocardium (end) and endothelium of dorsal aorta, intersomitic vessels, and yolk sac vessels. CD148 expression is also observed in the myocardium (myo) and midgut epithelium (mid). lu, lumen of yolk sac vessel. Competitive absorption with immunogen eliminates staining (c), and a class-matched mouse IgG shows no staining (d). (C) Confocal colocalization of CD31 and CD148 in dorsal aorta and adjacent intersomitic sprouts. Frozen embryo sections were double immunolabeled for CD148 (green) and CD31 (red) as described in Materials and Methods. Endothelial cells sprouting to intersomitic space expressed both CD31 (a) and CD148 (b). A merged image of the two stains shows overlapping expression of CD31 and CD148 in intersomitic endothelial cells (c). Note that homozygous mutant intersomitic vessels are enlarged and show reduced CD148 immunoreactivity (panel d, arrowheads). so, somites.

was incubated with anti-GFP mouse monoclonal antibody (Roche Applied Science) (10 μg/ml) overnight at 4°C and subsequently with protein G agarose for 2 h at 4°C. Positive control samples were prepared by immunoprecipitation of 100 μg of lysate protein from CHO cells transfected with expression plasmid pSRα or pSRα CD148$^{\Delta CyGFP}$. Bound proteins were washed three times in lysis buffer, boiled in sodium dodecyl sulfate sample buffer containing 10 mM dithiothreitol, separated by sodium dodecyl sulfate/polyacrylamide electrophoresis on 7.5% gels, and subjected to immunoblotting with anti-CD148 monoclonal antibody (clone Ab1 [1 μg/ml]) (45) or anti-GFP monoclonal antibody (Roche Applied Science) (1 μg/ml). For immunoabsorption experiments, the kidney tissue lysates were immunoprecipitated with either anti-GFP antibody (Roche Applied Science) (10 μg/ml) or mouse immunoglobulin G (IgG) (10 μg/ml) twice before incubation with wheat germ agarose beads.

**Whole-mount embryo immunostaining.** Procedures for whole-mount staining with anti-CD31, anti-endoglin, and anti-VEGFR2 (Flk1) antibodies were conducted as described previously (42). Briefly, the dissected embryos and yolk sacs were fixed in 4% paraformaldehyde–phosphate-buffered saline (PBS) for periods ranging from 1 h to overnight at 4°C. Then tissues were rinsed with PBS, dehydrated with methanol, bleached in 5% hydrogen peroxide–methanol, rehydrated, and blocked with PBSMT (2% instant milk, 0.2% Triton X-100 in PBS). Subsequently, the samples were incubated overnight with anti-CD31 monoclonal antibody (clone MEC 13.3 [Pharmingen]) (1.7 μg/ml), antiendoglin monoclonal antibody (clone MJ7/18 [Pharmingen]) (1.7 μg/ml), or anti-VEGFR2 antibody (clone Avas 12α1 [Pharmingen]) (1.7 μg/ml). The samples were then washed with PBSMT and incubated with horseradish peroxidase-conjugated F(ab′)$_2$ fragments of donkey anti-rat IgG (Jackson ImmunoResearch) (1 μg/ml) over-

night at 4°C. After washing with PBSMT and PBT (0.2% bovine serum albumin, 0.1% Triton X-100–PBS), the signals were developed in 0.3 mg of 3′3′-diaminobenzidine (DAB)/ml–0.5% $NiCl_2$–0.03% $H_2O_2$. The samples were postfixed with 2% paraformaldehyde–0.1% glutaraldehyde–PBS and then photographed. For CD148 labeling, the embryos were gently fixed in 4% paraformaldehyde–PBS (1 h at 4°C), incubated with CD148 monoclonal antibody (clone Ab1 [100 μg/ml]) overnight at 4°C (45) and then with fluorescein isothiocyanate-conjugated $F(ab')_2$ fragments of goat anti-mouse IgG (Jackson ImmunoResearch) (1 μg/ml) for 2 h at room temperature. The results were observed by confocal microscopy (Zeiss LSM410). For alpha smooth-muscle actin (αSMA) staining, the embryos and yolk sacs were fixed in methanol-dimethyl sulfoxide (4:1) overnight at 4°C, bleached, rehydrated, blocked, and incubated overnight with a horseradish peroxidase-conjugated anti-αSMA monoclonal solution (clone 1A4) (Enhanced Polymer System; DAKO).

**Histological evaluation.** Cold acetone-fixed cryostat sections of embryos and yolk sacs were immunostained using anti-CD148 monoclonal antibody (clone Ab1) and fluorescein isothiocyanate-conjugated $F(ab')_2$ fragments of goat anti-mouse IgG (Jackson ImmunoResearch) as previously described (45). In the double-labeling study for CD148 and CD31, rhodamine-conjugated anti-CD31 rat monoclonal antibody (clone MEC 13.3 [Pharmingen]) (5 μg/ml) was used. The results were analyzed by confocal microscopy (Zeiss LSM410). For analysis of whole-mount stained embryo sections, CD31- or αSMA-stained embryos were embedded in paraffin, sectioned on a microtome, and then counterstained with 1% alcohol–Eosin Y (Fisher HealthCare) or Nuclear Fast Red (DAKO). For Ki67 immunohistochemistry, 3% formalin-fixed paraffin sections of yolk sacs were treated in a microwave oven for 12 min in citrate buffer (pH 6) and incubated with anti-Ki67 goat polyclonal antibody (Santa Cruz Biotechnology) (2 μg/ml) for 1 h at room temperature and then the immunoreaction mixture was amplified using an ABC-Elite kit (Vector Laboratories). The immunoreactivity was color developed using 3′3′-DAB as a substrate (Liquid DAB Plus solution; DAKO), counterstained with Nuclear Fast Red (DAKO), and mounted. For morphometric analysis, yolk sac sections stained with hematoxylin and eosin were analyzed using image analysis software (Bioquant Corp., Nashville, Tenn.).

**Electron microscopy studies.** The yolk sacs were isolated from embryonic day 9.5 (E9.5) and 10.5 embryos, washed with PBS, and then fixed with Karnovsky's fixative (1.6% paraformaldehyde, 3% glutaraldehyde in 0.1 M sodium cacodylate buffer [pH 7.4]) for 1 h at 4°C. Tissues were then washed three times with washing buffer (3.5% sucrose in 0.1 M sodium cacodylate buffer [pH 7.3]), postfixed in buffered osmium tetroxide, and embedded in epoxy according to standard procedures. Ultrathin sections were stained in uranyl acetate and lead citrate and examined using a 100CX electron microscope operated at 60 kV (JEOL, Tokyo, Japan).

## RESULTS

**Generation of CD148 mutant mice.** To eliminate CD148 functions coupled to the cytoplasmic domain and tyrosine phosphatase activity, we designed a targeting vector that encodes a mutant allele, $CD148^{\Delta CyGFP}$, in which the C-terminal 117 amino acids (including the phosphatase domain) were replaced in frame by enhanced GFP sequences (Fig. 1A) (39). The CD148/GFP fusion protein encoded from the mutant allele included intact extracellular and transmembrane domains. Of 192 ES cell clones screened, two were used to establish independent lines of heterozygous recombinant mice with germ line transmission of the mutant allele. Since we noted the presence of a pseudogene during the present study (Fig. 1B), a correct targeting event was carefully confirmed. Both independent lines demonstrated expression of the CD148/GFP fusion mRNA transcripts by RT-PCR and Northern blot analysis (Fig. 1C) as well as that of a CD148/GFP fusion protein that also binds ectodomain interactive antibodies (Fig. 1D). A doublet of approximately 190 and 210 kDa was identified in kidney lysates by anti-CD148 immunoblotting following recovery with either WGA lectin (Fig. 1D, upper left panel) or anti-GFP (upper right panel). Anti-GFP antibodies identified fusion proteins of approximately 190 and 210 kDa recovered from heterozygous mutant animals by both approaches. Using anti-GFP and control IgG, a comparative immunoprecipitation study showed that the abundance of the mutant CD148/GFP was less than 50% of that of normal protein in the heterozygous kidney lysates (Fig. 1D), suggesting that the stability of the mutant protein had decreased. Depletion of the mutant CD148/GFP was confirmed by anti-GFP immunoblotting.

**$CD148^{\Delta CyGFP}$ homozygous mice die at midgestation.** The life expectancy, fertility, and gross appearance of the viable $F_1$ and $F_2$ heterozygous progeny appeared normal, yet no homozygous mutant mice were found among 130 offspring from heterozygous intercrosses. To confirm the embryonic lethality of the homozygous mutant mice, genotype analysis was performed at different embryonic stages on viable embryos ($n$ = 621) from heterozygous intercrosses. Homozygous mutant embryos at E8.5, 9.5, and 10.5 were recovered at Mendelian frequencies (E8.5, 28.4%; E9.5, 27.5%; E10.5, 25.0%), with complete loss of homozygous mutant embryos by E11.5. As early as E9.5, $CD148^{\Delta CyGFP}$ homozygous embryos were readily identified by growth retardation, smaller head size, absence of large branching vessels, and accumulation of primitive blood cells in the yolk sac. No differences were observed in somite numbers ($21.7 \pm 0.4$ [wild type] versus $21.4 \pm 0.4$ [homozygous mutant]) (Fig. 1E). By E10.5, the $CD148^{\Delta CyGFP}$ homozygous embryos displayed severe growth retardation and a prominently enlarged pericardial cavity (Fig. 1E). Identical findings were observed in homozygous mutant mice generated from each of the two independent ES clones and in homozygous mutant mice from which the floxed *neo* gene had been excised using a CRE-deleter mouse (EIIa-*cre* mice on a C57BL/6 background; provided by Mark Magnuson, Vanderbilt University). We also observed a shift in the ratio of viable wild-type to heterozygous embryos after E11.5 (44.9 versus 55.1%) coupled with resorption embryo remnants, suggesting that fetal demise occurred for a substantial fraction of heterozygous embryos in the 129/C57BL6 genetic background. The anatomic correlates of lethal outcome in these heterozygous embryos remain under investigation.

**CD148 is expressed in embryonic endothelial cells.** Using an ectodomain-interactive monoclonal antibody (45), we examined CD148 distribution in stage E9.0 embryos to determine the earliest sites of CD148 expression in developing embryos. Specific CD148 immunoreactivity was observed in vascular structures in intra- and extraembryonic sites, including the heart, dorsal aorta, intersomitic vessels, and yolk sac (Fig. 2A). Immunohistochemical analysis of E10.0 embryos revealed endocardial and endothelial distribution of CD148 in embryonic vasculature, including the dorsal aorta, intersomitic vessels, the umbilical artery, and the yolk sac vascular network (Fig. 2B). In addition, CD148 immunoreactivity was observed in developing myocardia, midgut epithelia, and in a subpopulation of hematopoietic cells (data not shown) (Fig. 2B, panel a). Specificity was confirmed by immunogen competition (45) and class-matched controls (Fig. 2B, panels c and d). Vascular structure immunostaining with anti-CD148 colocalized with CD31 (Fig. 2C, panel c) but not with αSMA (data not shown), consistent with vascular endothelium but not vSMC or PC expression.

It is noteworthy that the vascular endothelia of homozygous mutant embryo vessels show much weaker CD148 immunoreactivity with the ectodomain-interactive antibody that detects

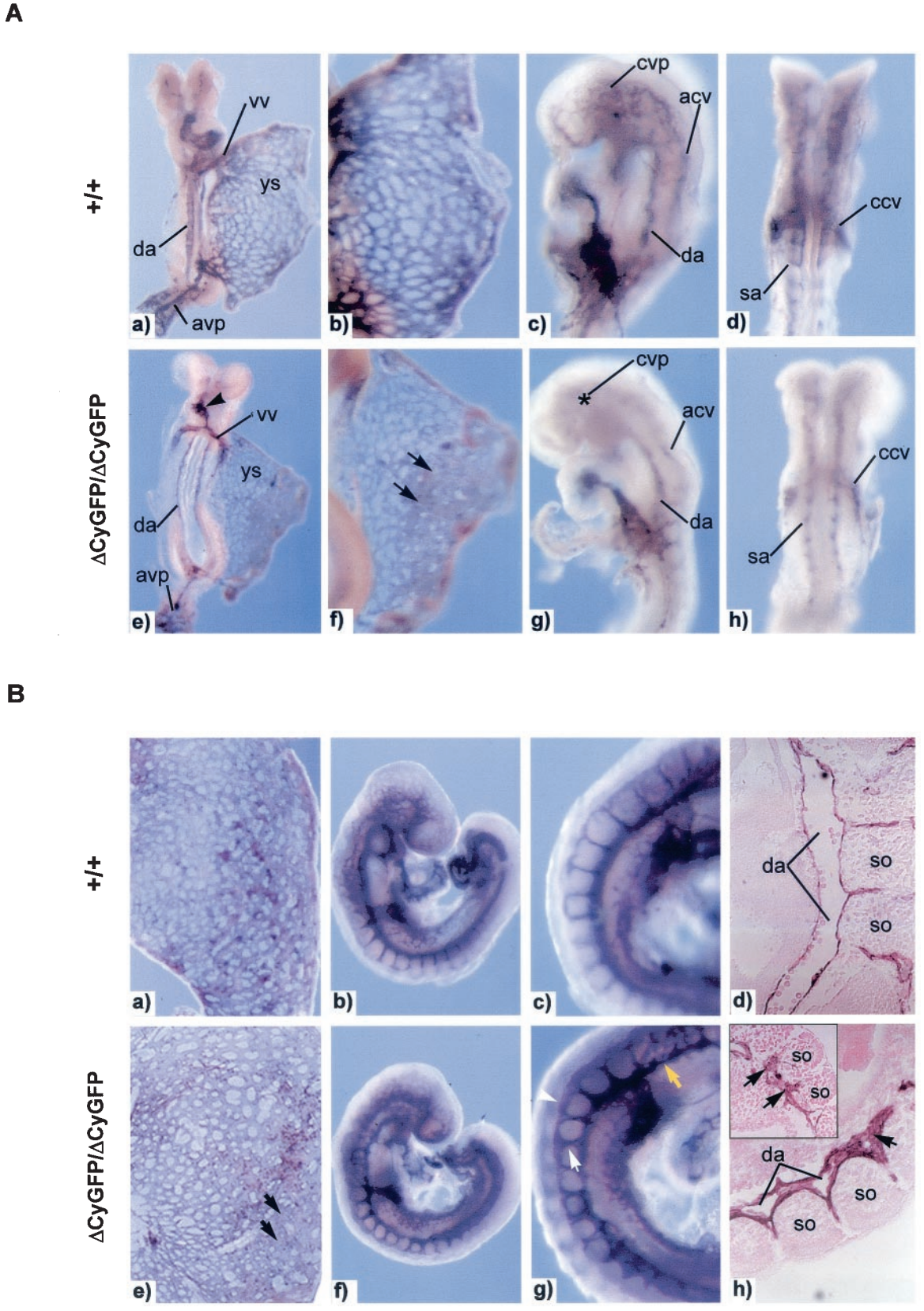


FIG. 3. Vascular development defects in CD148$^{\Delta CyGFP}$ homozygous embryos at E8.25 to 9.0. (A) Whole-mount CD31 immunostaining of E8.25 embryos. Embryos and yolk sacs were reconfigured into a planar format as previously described (15). The homozygous mutant embryos (e to h) exhibit delayed cardiac looping (panel e, arrowhead), focally enlarged yolk sac vessels (panel f, arrows), and poorly formed cerebral vascular plexus

the CD148/GFP fusion protein than those of wild-type vessels (Fig. 2C, panel d). This finding, coupled with those of reduced levels of the kidney lysate-derived CD148/GFP fusion protein (as detected by immunoblot analysis) and difficult-to-resolve GFP fluorescence in tissues from heterozygous mice, led us to infer that although expressed, the CD148/GFP fusion protein is short lived.

**Vascular development is defective in CD148$^{\Delta CyGFP}$ homozygous embryos.** The pattern of endothelial expression and the pericardial sac distention seen in homozygous mutant embryos prompted detailed examination of the cardiovascular system. We examined the structure of endothelial vessels by whole-mount immunostaining for the highly expressed endothelial surface marker, the platelet-endothelial cell adhesion molecule (CD31/PECAM1). At E8.25 to 8.5, homozygous mutant embryos were indistinguishable from wild-type embryos in the gross appearance of components of the central vascular tree, including the rostral-caudal dorsal aorta, anterior and posterior cardinal veins, vitelline artery and vein, and yolk sac capillary plexus (Fig. 3A). This finding suggests that CD148 is dispensable for early embryonic vasculogenesis and for the specification of angioblasts from the ventral mesoderm, their appropriate migration within the embryo, and their alignment to form the major vessels. However, upon closer inspection, subtler defects were noted as early as E8.25, including delayed heart looping (Fig. 3A, panel e), enlarged and fused yolk sac vessels (Fig. 3A, panel f), and a poorly formed cerebral vascular plexus (Fig. 3A, panel g).

By E9.0, a narrowed dorsal aortic trunk and enlarged intersomitic and intervertebral vessels were evident in homozygous mutant embryos (Fig. 3B, panel g). Analysis of CD31-stained sections from homozygous mutant embryos revealed collapse of the dorsal aorta accompanied by the presence of abundant endothelial cells with protruding extensions and enlarged intersomitic sprouts (Fig. 3B, panel h). Numbers of primitive hematopoietic cells in the homozygous mutant blood vessels at E8.25 to 9.0 appeared normal (data not shown). The allantois appeared to connect normally to the chorion in homozygous mutants, consistent with completion of the circuitry of the chorio-allantoic placental circulation.

In homozygous mutant mice at E9.5 to 10.5 (Fig. 4B), the dorsal aorta appeared as a disorganized string of aligned endothelial cells with fewer intersomitic sprouts (Fig. 4B, panel c); by E10.5, its outline was discontinuous (Fig. 4B, panel d). The cerebral vessels of homozygous mutant embryos lacked branching vessels of large diameters, consistent with a failure to remodel from the primary vascular plexus to hierarchically organized mature vessels (Fig. 4B, panel c). The peripheral vessels were expanded beyond normal dimensions, disordered, and densely interconnected (Fig. 4B, panels c and d). Histological sections of CD31-stained homozygous mutant embryos showed collapsed and atrophic dorsal aortae and oversized and disorganized peripheral vessels (Fig. 4C, panel d). No vascular abnormalities were detected in the heterozygous embryos examined between E8.25 and 10.5.

The extraembryonic circulation was similarly disrupted in CD148$^{\Delta CyGFP}$ homozygous mutant embryos. At E9.5, yolk sac vessels failed to mature and to form distinct vitelline vessels, remaining a meshwork of interconnected and homogeneously oversized endothelial cell-lined tubes (Fig. 4A, panel c). By E10.5, some further dilatation and endothelial compartment expansion was apparent, filling intercapillary spaces (Fig. 4A, panel d, and C, panel c). Histologically, the normal embryo pattern showed endothelial cell layers attached to the mesothelial and endodermal layers on opposite sides of the developing network (Fig. 4C, panel a, and D, panels a and b). In contrast, homozygous mutant vessels appeared to have expanded, displaying ill-defined contacts with mesothelial and endodermal layers (Fig. 4C, panel c). At E9.5, electron microscopic evaluation (Fig. 4D, panel c) showed gaps between endothelial cells of homozygous mutant yolk sac vessels. At E10.5, endothelial lined structures were detached from the mesothelial layer in some places (Fig. 4D, panel d). No dramatic difference was observed in hematopoietic colony formation for yolk sacs between heterozygous and homozygous mutant embryos (erythroid mean $\pm$ standard error of the mean [in CFU] in CD148$^{+/\Delta CyGFP}$, 112 $\pm$ 9 in CD148$^{+CyGFP/\Delta CyGFP}$ and 84 $\pm$ 12 in CD148$^{\Delta CyGFP/\Delta CyGFP}$; granulocyte and/or macrophage mean $\pm$ standard error of the mean, 37 $\pm$ 6 in CD148$^{+/\Delta CyGFP}$ and 25 $\pm$ 3 in CD148$^{\Delta CyGFP/\Delta CyGFP}$).

Morphometric analysis of yolk sac sections more clearly illustrated the processes responsible for the architectural disorganization. The homozygous mutant vessels were reduced in number (Fig. 5A) but showed an increase in the percentage of total vessels of larger diameters (i.e., those exceeding 800 $\mu m^2$) (Fig. 5B). Homozygous mutant yolk sacs showed a 58% increase in the number of endothelial cells per millimeter of vessel length, although the endodermal cell number did not differ significantly (Fig. 5C). This increased endothelial cell number suggested the presence of unregulated endothelial proliferation. This conclusion was further supported by the fact that homozygous mutant yolk sac endothelial cells more frequently presented as stained for Ki67, a nuclear protein expressed in proliferating cells (Fig. 5D). Terminal deoxynucleotidyltransferase-mediated dUTP-biotin nick end labeling staining showed no significant difference between wild-type and homozygous mutant yolk sacs in the numbers of apoptotic endothelial cells (data not shown). In the aggregate, the findings support a hypothesis of overactive endothelial prolifera-

(panel g, asterisk) compared with those of wild-type littermates (a to d). (a and e) Dorsal view; (b and f) close-up photograph of yolk sacs; (c and g) lateral view; (d and h) ventral view. Abbreviations: vv, vitelline vein; da, dorsal aorta; sa, somitic arteries; ys, yolk sac; avp, allantoic vascular plexus; cvp, cerebral vascular plexus; acv, anterior cardinal vein; ccv, common cardinal vein. (B) Whole-mount CD31 immunostaining of E9.0 embryos. Yolk sac vascular networks from a homozygous mutant (e) display homogenously sized and focally enlarged endothelial vessels (black arrows), while a wild-type littermate (a) displays differentiated vasculature composed of large- and small-diameter vessels of interconnecting cells. In the embryo proper, the homozygous mutant (f) is grossly similar to the wild type (b). Higher-magnification images (g) show a narrow dorsal aorta (yellow arrow) and enlarged intersomitic networks (white arrow) and dorsally fused (white arrowhead) intersomitic vessels. Sagittal sections of a CD31-stained homozygous mutant embryo (h) show a collapsed dorsal aorta which includes abundant endothelial cells (black arrows) and disorganized intersomitic sprouts (inset) compared with those of wild-type littermates (d). so, somite. Original magnification, $\times$200 (d and h).

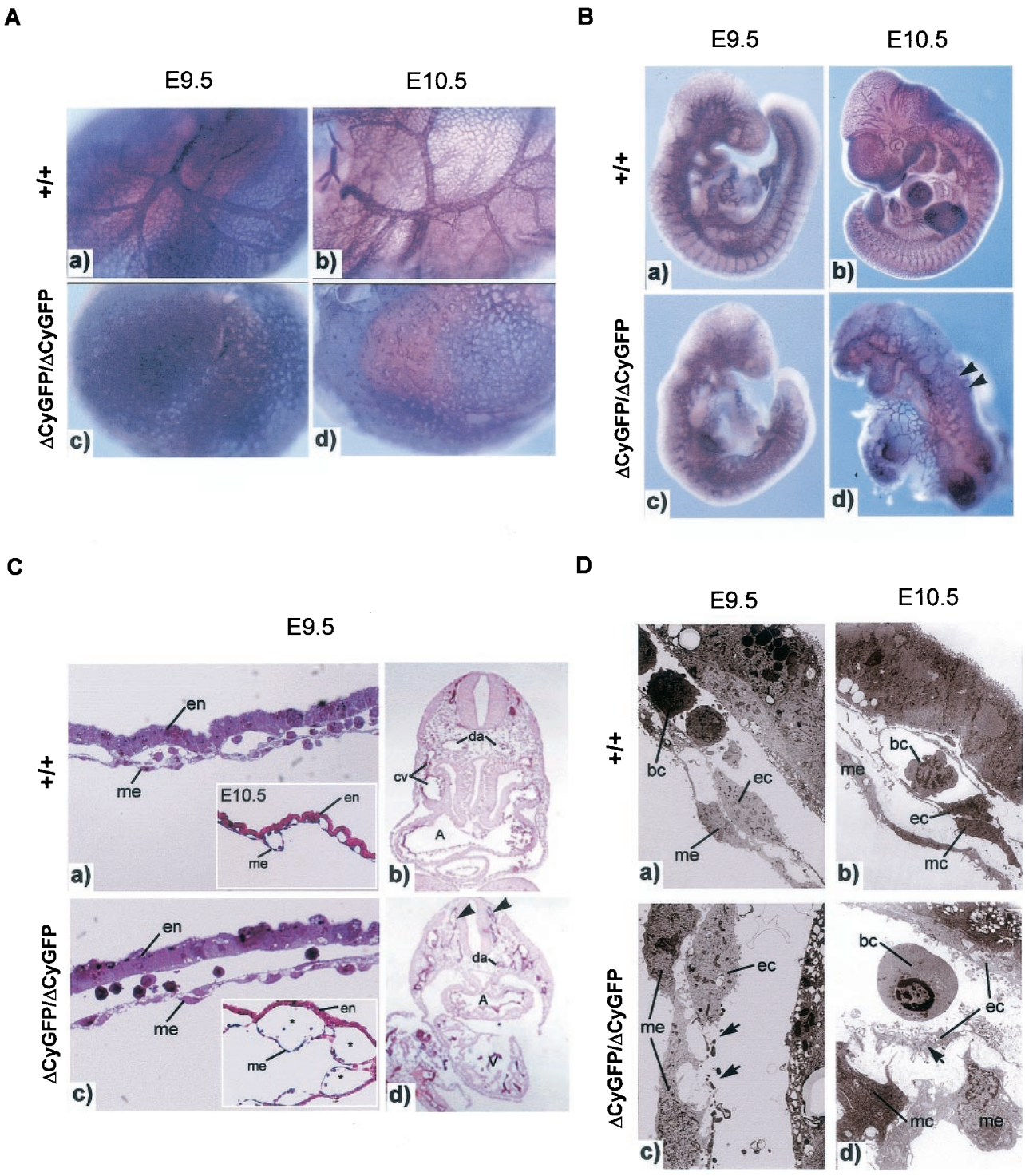


FIG. 4. Failure of vascular remodeling in CD148$^{\Delta CyGFP}$ homozygous embryos at E9.5 to 10.5. (A) Whole-mount CD31-immunolabeled yolk sacs at E9.5 to 10.5. Wild-type yolk sac vessels remodeled to form large vitelline vessels and a capillary network (a and b), in contrast to the expansion and fusion of endothelial structures in mutant yolk sac vessels (c and d). Few avascular areas were found between the vessels (c and d). (B) Whole-mount CD31 immunostaining of E9.5 to 10.5 embryos. Homozygous mutant embryos showed markedly disorganized vascular structure (c and d) compared with wild-type embryos (a and b). Dorsal aorta and intersomitic sprouts were not readily detectable, and peripheral vessels were enlarged and fused (panel d, arrowheads). (C) Histological sections of yolk sacs and embryos at E9.5 to 10.5. At E9.5, the capillary structure of wild-type yolk sacs was limited in size (a) whereas the homozygous mutant yolk sac displayed expanded vessels with a separation of the two endothelial layers (c). At E10.5, prominently dilated yolk sac vessels were observed in homozygous mutant embryo (panel c inset). Transverse sections of CD31-stained E9.5 homozygous mutant embryo show collapsed dorsal aorta and enlarged and disorganized peripheral vessels (panel d, arrowheads). Original magnification, ×20 (b and d). (a and b) Epon-embedded toluidine staining; (a and b insets and b and d) hematoxylin and eosin staining. en, endoderm; me, mesoepithelium; da, dorsal aorta; cv, cardinal vein; A, atrium; V, ventricle. (D) Electron micrographs of E9.5 to 10.5 yolk sacs. Homozygous mutant yolk sacs showed a discontinuity in the endothelial cells (panel c, arrows) at E9.5 and endothelial cellular detachment from subjacent mesoepithelium (panel d, arrow) at E10.5. me, mesoepithelium; mc, mural cells; ec, endothelial cells; bc, blood cells.

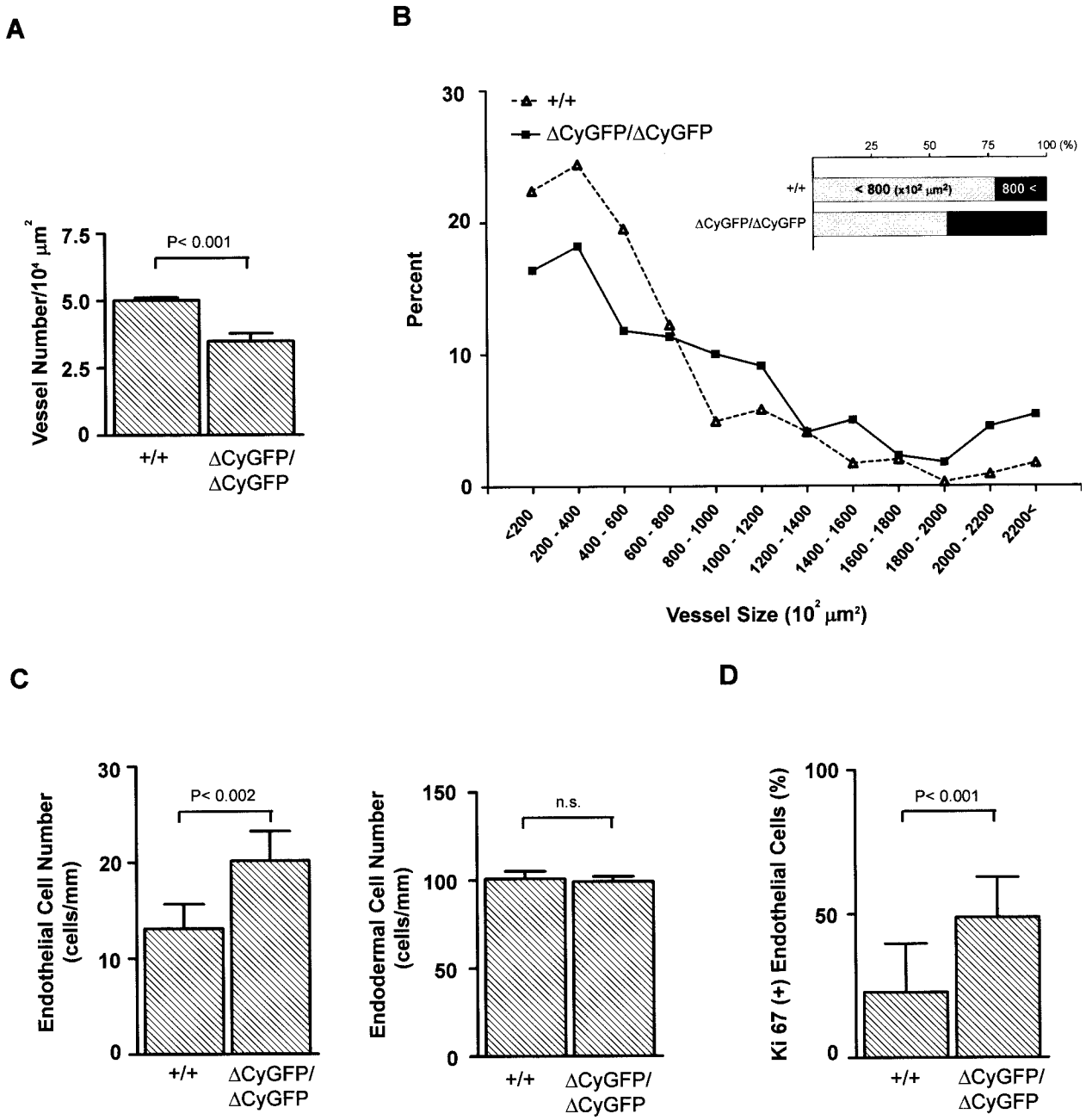


FIG. 5. Morphometric analysis of E9.0 yolk sac vasculature. (A) Vessel number in yolk sacs. The vessel number and the total tissue area were measured in sections of wild-type ($n = 3$) and homozygous mutant ($n = 3$) yolk sacs processed in parallel. A total of 15 sections per embryo were examined. (B) Distribution analysis assessing yolk sac vessel size. The intraluminal area of yolk sac vessels was measured in sections of wild-type ($n = 3$) and homozygous mutant ($n = 3$) yolk sacs processed in parallel. The homozygous mutant yolk sac vessels were enlarged (inset) and failed to form hierarchically organized vessels of different diameters. (C) Endothelial and endodermal cell numbers in yolk sacs. Endothelial cell (nuclei) number per millimeter of capillary length and number of endodermal cells (nuclei) lining yolk sac vessels were measured on sections from wild-type ($n = 3$) and homozygous mutant ($n = 3$) littermates. The homozygous mutant yolk sac vessels displayed increased endothelial cell numbers, while there was no difference in endodermal cell numbers. (D) Ki67 staining of yolk sac vessels. The frequency (percent) of endothelial cells labeled for Ki67 was calculated as described in Materials and Methods. The homozygous mutant yolk sac vessels displayed higher mitotic activity. Bars indicate the means ± standard errors of the means. Statistical analysis used an unpaired $t$ test.

tion and disordered endothelial-mesodermal contacts in mutant embryo yolk sacs.

**Cardiac defects in CD148$^{\Delta CyGFP}$ homozygous embryos.** Vascular anomalies were accompanied by heart defects in homozygous mutant embryos. At E9.0, CD31-stained homozygous mutant embryos showed delayed heart tube looping and aberrant endocardial projections while in wild-type littermates, CD31-stained endocardia were confined to the interior aspect of the heart tube (Fig. 6A, panels a and d). Confocal micrographs showed abnormal extensions of CD31-expressing endocardia

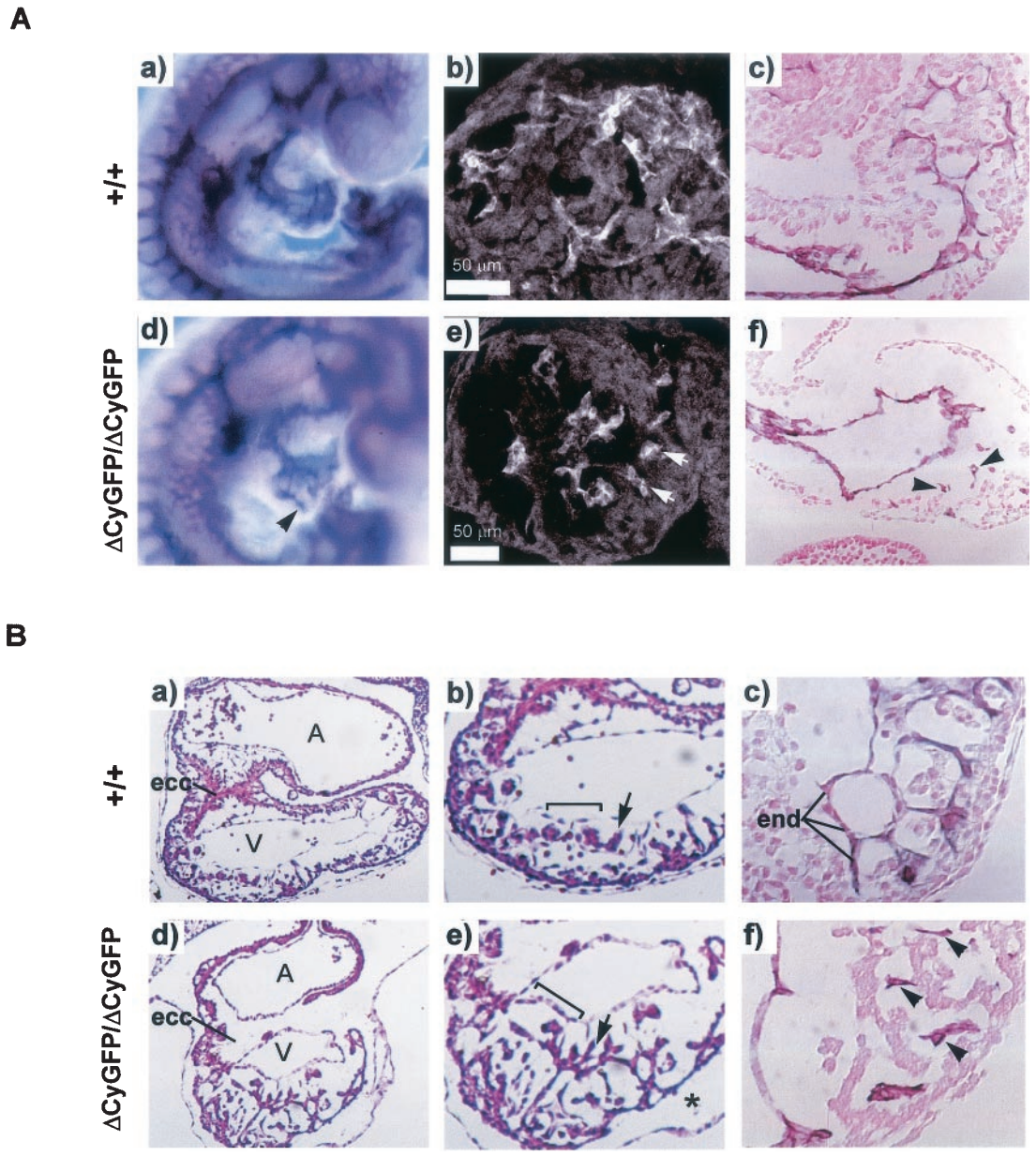


FIG. 6. Abnormal heart development in CD148$^{\Delta CyGFP}$ homozygous embryos. (A) CD31-stained cardiac tissue at E9.0. Homozygous mutant embryos show delayed heart looping accompanied by aberrant endocardial projections (panel d, arrowhead) compared to the wild-type embryo (a). Confocal sections of CD31-stained hearts show abnormal projections of homozygous mutant endocardium extending across the cardiac jelly space (panel e, white arrows), while the wild-type heart exhibited a continuous endocardial lining of the ventricular cavity (b). Sagittal sections of CD31-stained homozygous mutant hearts reveal rudimentary (less intricately folded) endocardium, scattered endocardial cells (panel f, arrowheads), and a decrease in the thickness of the myocardium and an absence of trabeculae (f) compared with those of a wild-type heart (c). Original magnification, ×80 (c and f). (B) Histological sections of E9.5 hearts. Sections of a homozygous mutant heart stained with hematoxylin and eosin (d) show disorganized myocardial trabeculation and defective endocardial cushion (ecc) formation. The wild-type myocardium formed finger-like trabeculae lined by endocardial cells (panel b, arrow), whereas homozygous mutant myocardial cells showed abnormal sprouts (panel e, arrow). The homozygous mutant endocardial cells showed rounded and shortened morphology (panel e, bracket) compared with wild-type endocardial cells (panel b, bracket). Note the enlarged pericardial cavity (panel e, asterisk) in the homozygous mutant heart. Sectional examination of CD31-stained homozygous mutant hearts showed a scattered and disconnected endocardial structure (panel f, arrowheads), while wild-type endocardia formed organized endocardial monolayers (panel c, end) tightly associated with myocardial trabeculae. A, atrium; V, ventricle. Original magnification, ×50 (a and d); ×100 (b and e); ×200 (c and f).

beyond the cardiac jelly, while wild-type endocardia showed continuous endocardial structure (Fig. 6A, panels b and e). Transverse sections of the homozygous mutant hearts revealed less-intricately-folded endocardia and scattered, disconnected endocardial cells compared with those of wild-type littermates (Fig. 6A, panels c and f). Homozygous mutants showed decreased thickness of the myocardial wall, coupled with increased space between the endocardium and myocardium, im-

plying the presence of either greater amounts of cardiac jelly between the two heart layers or collapsed endocardia (Fig. 6A, panel f). At E9.5, normal embryos showed signs of a progressively developing endocardium, such as increasing trabeculation and closure of the atrioventricular canal by the formation of endocardial cushion (Fig. 6B, panels a through c). In contrast, the homozygous mutant embryos displayed disorganized trabeculation, lacking finger-like trabeculae lined by endocardial cells (Fig. 6B, panel e). Endocardia were discontinuous (Fig. 6B, panels e and f), and developing hearts lacked mesenchymal cushion formation adjacent to the atrioventricular canal (Fig. 6B, panel d).

**Impaired perivascular cell investment and reduced endoglin expression in CD148$^{\Delta CyGFP}$ homozygous vasculature.** vSMCs and PCs critically regulate endothelial cell proliferation and migration and vascular remodeling (21). The increased endothelial cell number and the failure of vascular remodeling led us to further examine vSMC-PC development in the homozygous mutant embryos. We examined vSMC-PC formation by performing whole-mount immunostaining for αSMA. At E9.0 to 9.5, αSMA expression was observed in perivascular regions of yolk sac endothelial capillaries in both wild-type and homozygous mutant embryos, though there seemed to be a slight decrease in the number of vSMCs and PCs in homozygous mutant yolk sacs at E9.0 (Fig. 7A, panels a through d). As shown in Fig. 7A, panels a and c, vSMCs and PCs are circumferentially arranged and tightly associated with the endothelium in the wild-type yolk sac. In contrast, vSMCs and PCs are poorly elongated and loosely invest adjacent endothelial vessels in homozygous mutant yolk sacs. Examination of αSMA-stained yolk sac sections identified vSMCs and PCs between the endoderm and endothelium in both wild-type and homozygous mutant yolk sacs. However, vSMCs and PCs on the homozygous mutant yolk sac vessels were sparsely distributed and displayed rounded morphology (Fig. 7A, panels e and f). In the embryo proper, αSMA expression was observed in the heart, dorsal aorta, and myotome of the somites in wild-type embryos at E10.0 (Fig. 7A, panel g). In contrast, homozygous mutant embryos revealed a dramatic reduction of αSMA expression in the dorsal aorta and somites (Fig. 7A, panel h). Consistent with the results of whole-mount staining, αSMA immunohistochemistry exhibited few vSMCs around the homozygous mutant dorsal aorta (data not shown).

To dissect the molecular events underlying the failed vascular remodeling and vSMC-PC investment, we examined by whole-mount immunostaining the expression of pivotal molecules known to be involved in vascular remodeling. These include VEGFR2 (Flk1), Tie2, Tal1/SCL, VE-cadherin, endoglin (CD105), and ALK1. We further examined the expression of ephrin-B2 by introducing an ephrin-B2$^{tlacZ}$ allele into CD148$^{\Delta CyGFP}$ homozygous embryos using ephrin-B2$^{tlacZ/+}$ mice (49). Expression of endoglin, an integral membrane glycoprotein that binds to members of the TGFβ superfamily and associates with other TGFβ receptors (3), was greatly reduced throughout the entire vasculature in homozygous mutant embryos (Fig. 7B), while the expression of other molecules, as represented by VEGFR2 expression, was unaffected (Fig. 7B). In CD148$^{\Delta CyGFP}$ homozygous embryos, ephrin-B2 promoter activity was observed in normal patterns in arterial vascular structures, including endocardium, dorsal aorta and its intersomitic sprouts, as well as in the subpopulation of yolk sac endothelial cells. Yolk sac expression of VEGF-A, angiopoietins 1 and 2, PDGF-B, PDGFβ receptor, TGFβ-1 and -2, TGFβ type I and II receptors, ALK1, D*ll* 1 and 4, and Notch1 and -4, was examined at E9.0 to 9.5 by RT-PCR analysis. Among these transcripts, only levels of VEGF-A were increased (5- to 10-fold) in homozygous mutant yolk sacs, a finding consistent with hypoxic consequences of vascularization failure (38) or, plausibly, a more direct effect of the lack of a functional CD148 receptor tyrosine phosphatase.

## DISCUSSION

In the present study, we demonstrated that a receptor tyrosine phosphatase, CD148, is required for vascular development. Mice homozygous for a phosphatase-inactivating CD148 mutation die before E11.5 with prominent growth retardation accompanied by both intra- and extraembryonic vascular anomalies that correlate with the timing and distribution of CD148 expression. Increased proliferation and expansion of the endothelial cell compartment expressing CD148 are components of the mutant phenotype and are consistent with CD148 effects to mediate growth inhibition (27, 43, 47). Another component of the phenotype is the defective vascular remodeling and association of vSMCs or PCs with endothelium-lined vessels. This is similar to a feature in endoglin-deficient embryos (32) and is associated with reduced endoglin expression in the homozygous CD148 mutant embryos (Fig. 7B).

It is a challenge to discriminate primary effects of genetic mutations in vascularization-defective embryos from secondary effects of circulatory failure and ischemia. Findings that the vascular phenotypes correlate temporally with the onset of CD148 expression and that these phenotypes also precede the developmental onset of a functional circulation are attributable to primary effects of the mutation. In normal yolk sac endothelial progenitor cells, CD148 expression is evident by E8.25 (data not shown). In homozygous mutant embryos, a normal early sequence of endothelial differentiation is seen, marked by normal expression (by E7.5) of the angioblast marker TAL1/SCL (14, 15) and by subsequent expression of Flk1, CD31, Tie2, ephrin-B2, and VE-cadherin (data not shown). Despite this intact developmental molecular sequence, yolk sac vascular plexus abnormalities were noted as early as E8.25 (Fig. 3A), at a stage when endothelial progenitors are engaged in de novo vessel formation (vasculogenesis) (15). This developmental window precedes initiation of cardiac contractile activity in normal embryos (E8.5 to 9.0) and suggests the presence of altered endothelial behaviors in homozygous mutant embryos.

The increased proliferative index of the endothelial progenitor compartment (Fig. 5) supports an important role of CD148 in attenuating proliferation of endothelial progenitors, as it does in other cell types (27, 47). Further evidence for a primary defect in regulation of endothelial progenitor proliferation has been provided by an independent evaluation of embryoid bodies derived from homozygous CD148$^{\Delta CyGFP}$ mutant ES lines (50). We found that homozygous mutant ES lines generated embryoid bodies containing twofold increased numbers of CD31-positive endothelial cells per total

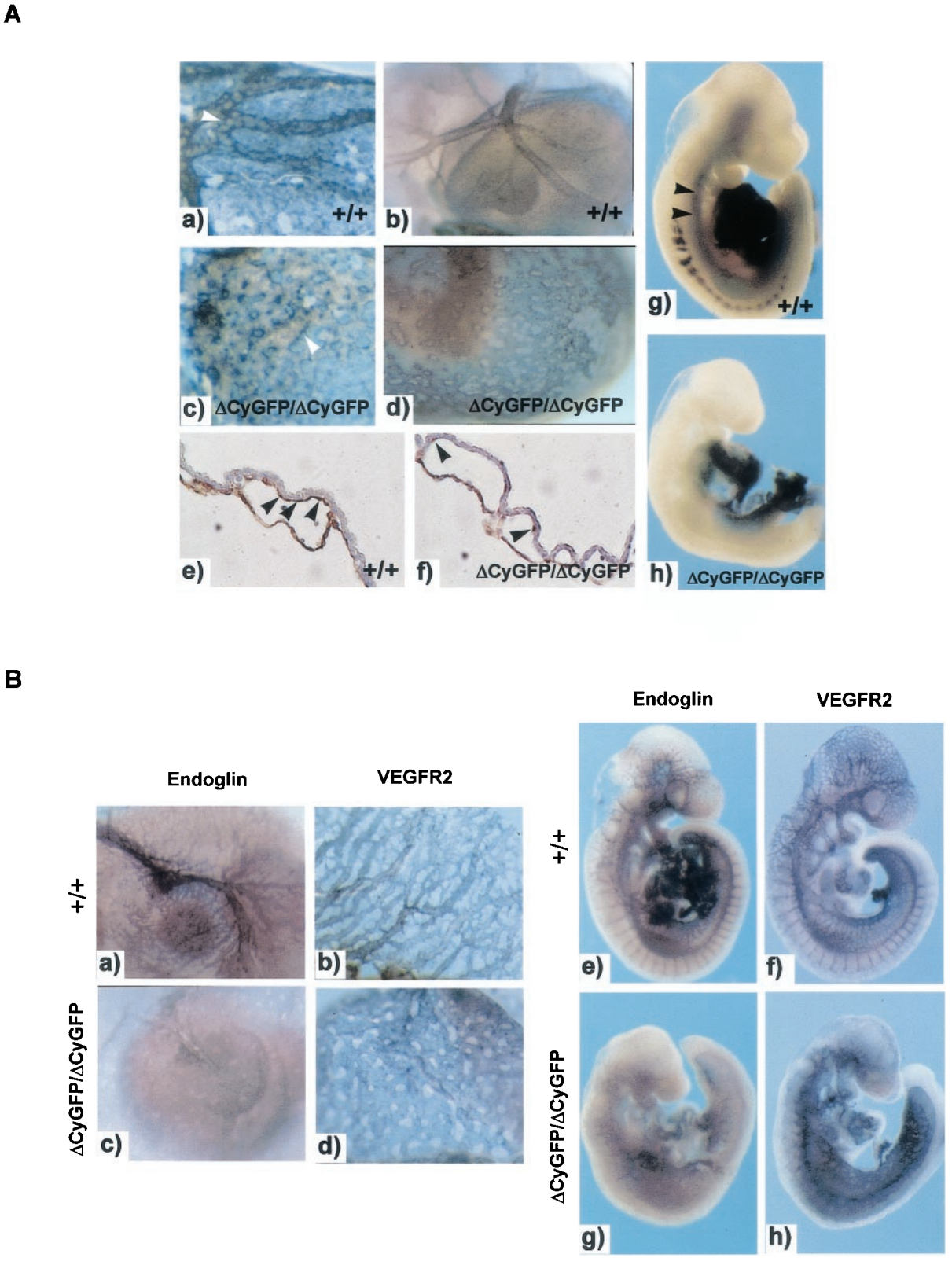


FIG. 7. Impaired perivascular cell investment and reduced vascular endoglin expression in CD148$^{\Delta CyGFP}$ homozygous embryos. (A) Whole-mount αSMA immunostaining of E9.0 to 9.5 embryos. The αSMA-positive perivascular cells (vSMC and PC) were observed around endothelial tubes in both wild-type and homozygous mutant yolk sacs at E9.0 (a and c) and 9.5 (b and d). In wild-type yolk sacs, vSMCs and PCs are circumferentially arranged and tightly associated with the endothelial vessels (panel a, white arrowhead), whereas vSMCs and PCs fail to encircle the vessels and are loosely associated with the endothelium in homozygous mutant yolk sacs (panel c, white arrowhead). (e and f) Sections of E9.0 yolk sacs immunostained for αSMA. CD148$^{\Delta CyGFP/\Delta CyGFP}$ yolk sacs show round and sparsely distributed vSMCs and PCs between the endoderm

cells at days 4 and 8 (24% in $CD148^{+/\Delta CyGFP}$ and 42% in $CD148^{\Delta CyGFP/\Delta CyGFP}$ at day 4). On the other hand, proliferative features of the homozygous mutant endothelia might reflect effects of a local hypoxic microenvironment compromised by circulatory failure. Quantitative RT-PCR analysis of VEGF-A transcripts in homozygous mutant yolk sacs at E9.0 demonstrated 5- to 10-fold up-regulation (data not shown), matching similar observations in other knockouts displaying embryonic vascular lethal phenotypes (5, 38). Increased endothelial proliferation and vascular enlargement are anticipated consequences of local VEGF induction (16), yet it appears that the expansion of the endothelial compartment of $CD148^{\Delta CyGFP}$ homozygous embryos precedes this reactive VEGF induction and exceeds that seen in other embryonic vascular lethal mutants (5, 38). In the aggregate, we anticipate that the endothelial compartment expansion seen in the homozygous mutant embryos reflects summation of two combined influences: (i) loss of cell autonomous growth regulation from the disabling of the CD148 tyrosine phosphatase and (ii) prolonged and amplified endothelial proliferation stimulated by hypoxia-VEGF excess.

Previous findings have implicated CD148 in cell-cell interactions. We previously observed that CD148 accumulates in cultured endothelial cells and in mature arterial vessels at sites of interendothelial contact, although it is not restricted to those sites (45). Originally named density-enhanced phosphatase (DEP-1), CD148 was reported to increase in abundance in densely packed cultured cells (36). In this study, electron micrographs of homozygous mutant yolk sacs displayed discontinuous interconnections between endothelial cells and subjacent supportive cells (Fig. 4D). Similarly, cardiomyocytes expressed CD148 at early developmental stages (Fig. 2B) and displayed disorganized trabeculation. Evidence from homozygous mutant embryos supports the possibility that the CD148 mutation impairs initiation and/or maturation of primary cell-cell contacts. Alternatively, the increased rate of endothelial proliferation might outpace the formation of normal intercellular contacts with subjacent cells. The CD148 ectodomain does not mediate the homophilic intercellular adhesion seen with PTPμ and PTPκ receptor phosphatases (9, 41) (unpublished results), yet some downstream events requiring phosphatase function are needed to drive assembly and maturation of interactions between endothelial cells.

Since a functional ligand for CD148 has not yet been identified, it is unclear whether localized accumulation at intercellular contact points reflects engagement of the CD148 ectodomain with an ectodomain binding partner expressed on contacting cells or whether the accumulation is the consequence of other molecular interactions. With the caveat that the expressed CD148/GFP fusion protein is less stable than native CD148, the evidence suggests that the tyrosine phosphatase activity of CD148 is functionally coupled to endothelial growth regulation. A further comparative study with the null mutation embryo is required to validate the impact of CD148 catalytic dysfunction on the phenotype.

A number of molecular induction events are required for normal developmental vascular remodeling at E9.5 to 10.5 (10, 22). At the cellular level, this remodeling is coordinated between endothelial cells and peri-vSMCs and PCs. Impaired association of vSMCs and PCs with endothelial cells in the homozygous mutant yolk sacs (Fig. 7A) suggests that the mutation interrupts responsible growth factors. However, homozygous mutant embryos showed no detectable changes in abundance of transcripts for two distinct growth factor and receptor systems implicated in these events, PDGF-B/PDGFβ receptors and TGFβ-1/TGFβ receptors (22) (data not shown). Within the embryo proper, the number of αSMA-positive cells was reduced in the homozygous mutants (Fig. 7A). It is uncertain whether this was a consequence of loss of endothelium-derived signals supporting vSMC-PC differentiation or secondary to circulatory compromise and ischemia. This difference between extraembryonic sites where vSMC-PC numbers are normal and intraembryonic sites where they are reduced is consistent with relatively delayed timing of intraembryonic vSMC-PC differentiation (E9.5 versus E8.5) (46). In the aggregate, we interpret these effects on the vSMC-PC compartment to be secondary consequences of the primary effects of CD148 upon the endothelial compartment.

The CD148 homozygous mutant embryos failed to express endoglin at the normal developmental stage (Fig. 7B). Endoglin is predominantly expressed in vascular endothelial cells and in the endocardium during embryogenesis (24). Endoglin-deficient mice die by E11.5 due to defective vascular development accompanied by (i) reduction in vSMC-PC compartment expansion and capillary incorporation and (ii) failure of endocardial-mesenchymal transformation and endocardial cushion formation (8, 32). Despite the effects of the CD148 mutation in inhibiting endoglin expression and evoking defects similar to those in endoglin-deficient embryos, some of the CD148 mutant phenotype features are distinct. For example, endothelium-lined vascular structures are already disorganized in $CD148^{\Delta CyGFP}$ homozygous embryos by E9.5 (Fig. 4), a time when they appear structurally intact in endoglin-deficient embryos (32). Inhibition of endoglin expression enhances the ability of TGFβ-1 to suppress endothelial growth and migration (31), and anti-endoglin antibodies inhibit tumor angiogenesis (44). These findings support a role for endoglin in the promotion of endothelial proliferation and migration through TGFβ receptor signaling. While it appears likely that the CD148 mutation effects on endoglin expression contribute to the phenotype, antiproliferative effects of CD148 overexpression are seen in cell types not expressing endoglin, arguing that CD148 has independent roles in regulating endothelial proliferation.

and endothelium (panel f, arrowheads), while vSMCs and PCs encircle endothelial vessels in wild-type yolk sacs (panel e, arrowheads). Original magnification, ×400 (e and f). In the embryo proper, whole-mount αSMA staining at E10.0 showed obviously reduced αSMA expression around the dorsal aorta in the homozygous mutant (h) compared with that of the wild type (arrowheads, g). (B) Whole-mount immunostaining for endoglin and VEGFR2 (Flk1) at E9.5. Endoglin expression was down-regulated in the homozygous mutant yolk sac and intraembryonic vessels (c and g) compared with that seen in those of the wild-type embryo (a and e); similar levels of VEGFR2 expression were observed in wild-type (b and f) and homozygous mutant (d and h) vasculature.

CD148 is expressed for a range of hematopoietic lineages (12), raising the question of whether lineage potential other than the endothelial was affected in the CD148 mutants. In this context, similar numbers of blood cells were identified in vessels of homozygous mutant compared with those of normal embryos prior to E11.5. Immunostaining with TAL1/SCL, a marker for primitive hematopoiesis (4, 26), displayed similar levels of expression in the homozygous mutant embryos (data not shown). Further, there was no difference in hematopoietic colony formation of yolk sac between heterozygous and homozygous mutant embryos. Thus, available data speak against effects of this CD148 mutation upon the hematopoietic compartment.

Our strategy was designed to permit resolution of the mutant $CD148^{\Delta CyGFP}$ protein by GFP. Expression of single-copy GFP gene fusions has been sufficient to permit detection in several mutant lines (19, 25), yet the CD148/GFP fusion protein was not resolved in situ by confocal microscopy. Comparative immunoblot and immunostaining evidence (Fig. 1D and 2C) supports the possibility that the CD148/GFP fusion protein is expressed from the homologous recombinant allele, but its instability makes it difficult to detect. Whether other features of the fusion protein or its interactions impair GFP fluorescence is unknown.

In conclusion, the present study indicates an indispensable role for CD148 catalytic function in vascular development through the regulation of endothelial cell growth and endothelium-PC interaction. The ability to activate or repress CD148 function would be a new tool to manipulate the processes of neovascularization.

## ACKNOWLEDGMENTS

We thank Brigid Hogan for valuable discussions and invaluable experimental method instruction, Stephen J. Brandt for providing anti-Tal1/SCL antibody, and Cathy Pettepher, Tsutom Kume, Keita Hirano, and Cornelia Crooke for technical assistance. We also thank the Francis Willams Preston Transgenic Mouse/ES Cell Shared Resource, supported by Cancer Center Support Grant P30 CA 68485 and Diabetes Center Support Grant P60 DK 20593, for screening and microinjection of ES cells. Analysis was performed in part through use of the VICC Cell Imaging Resource supported by CA68485 and DK20593.

This work was supported by grants from the National Institutes of Health (DK38517 to T.O.D. and DK52483 to D.R.A.) and the Juvenile Diabetes Foundation (2-2000-147 to T. Takahashi).

## REFERENCES

1. **Adams, R. H.** 2002. Vascular patterning by Eph receptor tyrosine kinases and ephrins. Semin. Cell Dev. Biol. **13:**55–60.
2. **Baker, J. E., R. Majeti, S. G. Tangye, and A. Weiss.** 2001. Protein tyrosine phosphatase CD148-mediated inhibition of T-cell receptor signal transduction is associated with reduced LAT and phospholipase Cγ1 phosphorylation. Mol. Cell. Biol. **21:**2393–2403.
3. **Barbara, N. P., J. L. Wrana, and M. Letarte.** 1999. Endoglin is an accessory protein that interacts with the signaling receptor complex of multiple members of the transforming growth factor-beta superfamily. J. Biol. Chem. **274:**584–594.
4. **Begley, C. G., P. D. Aplan, S. M. Denning, B. F. Haynes, T. A. Waldmann, and I. R. Kirsch.** 1989. The gene SCL is expressed during early hematopoiesis and encodes a differentiation-related DNA-binding motif. Proc. Natl. Acad. Sci. USA **86:**10128–10132.
5. **Bi, W., C. J. Drake, and J. J. Schwarz.** 1999. The transcription factor MEF2C-null mouse exhibits complex vascular malformations and reduced cardiac expression of angiopoietin 1 and VEGF. Dev. Biol. **211:**255–267.
6. **Bianchi, C., F. W. Sellke, R. L. Del Vecchio, N. K. Tonks, and B. G. Neel.** 1999. Receptor-type protein-tyrosine phosphatase mu is expressed in specific vascular endothelial beds in vivo. Exp. Cell Res. **248:**329–338.
7. **Borges, L. G., R. A. Seifert, F. J. Grant, C. E. Hart, C. M. Disteche, S. Edelhoff, F. F. Solca, M. A. Lieberman, V. Lindner, E. H. Fischer, S. Lok, and D. F. Bowen-Pope.** 1996. Cloning and characterization of rat density-enhanced phosphatase-1, a protein tyrosine phosphatase expressed by vascular cells. Circ. Res. **79:**570–580.
8. **Bourdeau, A., D. J. Dumont, and M. Letarte.** 1999. A murine model of hereditary hemorrhagic telangiectasia. J. Clin. Investig. **104:**1343–1351.
9. **Brady-Kalnay, S. M., D. L. Rimm, and N. K. Tonks.** 1995. Receptor protein tyrosine phosphatase PTPμ associates with cadherins and catenins in vivo. J. Cell Biol. **130:**977–986.
10. **Carmeliet, P.** 2000. Mechanisms of angiogenesis and arteriogenesis. Nat. Med. **6:**389–395.
11. **Daniel, T. O., and D. Abrahamson.** 2000. Endothelial signal integration in vascular assembly. Annu. Rev. Physiol. **62:**649–671.
12. **de la Fuente-Garcia, M. A., J. M. Nicolas, J. H. Freed, E. Palou, A. P. Thomas, R. Vilella, J. Vives, and A. Gaya.** 1998. CD148 is a membrane protein tyrosine phosphatase present in all hematopoietic lineages and is involved in signal transduction on lymphocytes. Blood **91:**2800–2809.
13. **Desai, C. J., Q. Sun, and K. Zinn.** 1997. Tyrosine phosphorylation and axon guidance: of mice and flies. Curr. Opin. Neurobiol. **7:**70–74.
14. **Drake, C. J., S. J. Brandt, T. C. Trusk, and C. D. Little.** 1997. TAL1/SCL is expressed in endothelial progenitor cells/angioblasts and defines a dorsal-to-ventral gradient of vasculogenesis. Dev. Biol. **192:**17–30.
15. **Drake, C. J., and P. A. Fleming.** 2000. Vasculogenesis in the day 6.5 to 9.5 mouse embryo. Blood **95:**1671–1679.
16. **Drake, C. J., A. LaRue, N. Ferrara, and C. D. Little.** 2000. VEGF regulates cell behavior during vasculogenesis. Dev. Biol. **224:**178–188.
17. **Fachinger, G., U. Deutsch, and W. Risau.** 1999. Functional interaction of vascular endothelial-protein-tyrosine phosphatase with the angiopoietin receptor Tie-2. Oncogene **18:**5948–5953.
18. **Ferrara, N.** 2001. Role of vascular endothelial growth factor in regulation of physiological angiogenesis. Am. J. Physiol. Cell Physiol. **280:**C1358–C1366.
19. **Godwin, A. R., H. S. Stadler, K. Nakamura, and M. R. Capecchi.** 1998. Detection of targeted GFP-Hox gene fusions during mouse embryogenesis. Proc. Natl. Acad. Sci. USA **95:**13042–13047.
20. **Hadjantonakis, A. K., M. Gertsenstein, M. Ikawa, M. Okabe, and A. Nagy.** 1998. Generating green fluorescent mice by germline transmission of green fluorescent ES cells. Mech. Dev. **76:**79–90.
21. **Hellstrom, M., H. Gerhardt, M. Kalen, X. Li, U. Eriksson, H. Wolburg, and C. Betsholtz.** 2001. Lack of pericytes leads to endothelial hyperplasia and abnormal vascular morphogenesis. J. Cell Biol. **153:**543–553.
22. **Hirschi, K. K., S. A. Rohovsky, and P. A. D'Amore.** 1997. Cell-cell interactions in vessel assembly: a model for the fundamentals of vascular remodelling. Transplant Immunol. **5:**177–178.
23. **Jones, N., K. Iljin, D. J. Dumont, and K. Alitalo.** 2001. Tie receptors: new modulators of angiogenic and lymphangiogenic responses. Nat. Rev. Mol. Cell Biol. **2:**257–267.
24. **Jonker, L., and H. M. Arthur.** 2002. Endoglin expression in early development is associated with vasculogenesis and angiogenesis. Mech. Dev. **110:**193–196.
25. **Jung, S., J. Aliberti, P. Graemmel, M. J. Sunshine, G. W. Kreutzberg, A. Sher, and D. R. Littman.** 2000. Analysis of fractalkine receptor $CX_3CR1$ function by targeted deletion and green fluorescent protein reporter gene insertion. Mol. Cell. Biol. **20:**4106–4114.
26. **Kallianpur, A. R., J. E. Jordan, and S. J. Brandt.** 1994. The SCL/TAL-1 gene is expressed in progenitors of both the hematopoietic and vascular systems during embryogenesis. Blood **83:**1200–1208.
27. **Keane, M. M., G. A. Lowrey, S. A. Ettenberg, M. A. Dayton, and S. Lipkowitz.** 1996. The protein tyrosine phosphatase DEP-1 is induced during differentiation and inhibits growth of breast cancer cells. Cancer Res. **56:**4236–4243.
28. **Krebs, L. T., Y. Xue, C. R. Norton, J. R. Shutter, M. Maguire, J. P. Sundberg, D. Gallahan, V. Closson, J. Kitajewski, R. Callahan, G. H. Smith, K. L. Stark, and T. Gridley.** 2000. Notch signaling is essential for vascular morphogenesis in mice. Genes Dev. **14:**1343–1352.
29. **Kume, T., T. Watanabe, R. Sanokawo, D. Chida, T. Nakamura, and M. Oishi.** 1996. Expression of the protein tyrosine phosphatase β2 gene in mouse erythroleukemia cells induces terminal erythroid differentiation. J. Biol. Chem. **271:**30916–30921.
30. **Kuramochi, S., S. Matsuda, Y. Matsuda, T. Saitoh, M. Ohsugi, and T. Yamamoto.** 1996. Molecular cloning and characterization of Byp, a murine receptor-type tyrosine phosphatase similar to human DEP-1. FEBS Lett. **378:**7–14.
31. **Li, C., I. N. Hampson, L. Hampson, P. Kumar, C. Bernabeu, and S. Kumar.** 2000. CD105 antagonizes the inhibitory signaling of transforming growth factor β1 on human vascular endothelial cells. FASEB J. **14:**55–64.
32. **Li, D. Y., L. K. Sorensen, B. S. Brooke, L. D. Urness, E. C. Davis, D. G. Taylor, B. B. Boak, and D. P. Wendel.** 1999. Defective angiogenesis in mice lacking endoglin. Science **284:**1534–1537.
33. **Lindahl, P., H. Bostrom, L. Karlsson, M. Hellstrom, M. Kalen, and C. Betsholtz.** 1999. Role of platelet-derived growth factors in angiogenesis and alveogenesis. Curr. Top. Pathol. **93:**27–33.

34. **Oh, S. P., T. Seki, K. A. Goss, T. Imamura, Y. Yi, P. K. Donahoe, L. Li, K. Miyazono, P. ten Dijke, S. Kim, and E. Li.** 2000. Activin receptor-like kinase 1 modulates transforming growth factor-beta 1 signaling in the regulation of angiogenesis. Proc. Natl. Acad. Sci. USA **97:**2626–2631.
35. **Oshima, M., H. Oshima, and M. M. Taketo.** 1996. TGF-beta receptor type II deficiency results in defects of yolk sac hematopoiesis and vasculogenesis. Dev. Biol. **179:**297–302.
36. **Ostman, A., Q. Yang, and N. K. Tonks.** 1994. Expression of DEP-1, a receptor-like protein-tyrosine-phosphatase, is enhanced with increasing cell density. Proc. Natl. Acad. Sci. USA **91:**9680–9684.
37. **Papetti, M., and I. M. Herman.** 2002. Mechanisms of normal and tumor-derived angiogenesis. Am. J. Physiol. Cell Physiol. **282:**C947–C970.
38. **Pereira, F. A., Y. Qiu, G. Zhou, M. J. Tsai, and S. Y. Tsai.** 1999. The orphan nuclear receptor COUP-TFII is required for angiogenesis and heart development. Genes Dev. **13:**1037–1049.
39. **Piston, D. W., G. H. Patterson, and S. M. Knobel.** 1999. Quantitative imaging of the green fluorescent protein (GFP). Methods Cell Biol. **58:**31–48.
40. **Ruivenkamp, C. A., T. Van Wezel, C. Zanon, A. P. Stassen, C. Vlcek, T. Csikos, A. M. Klous, N. Tripodis, A. Perrakis, L. Boerrigter, P. C. Groot, J. Lindeman, W. J. Mooi, G. A. Meijjer, G. Scholten, H. Dauwerse, V. Paces, N. Van Zandwijk, G. J. Van Ommen, and P. Demant.** 2002. Ptprj is a candidate for the mouse colon-cancer susceptibility locus Scc1 and is frequently deleted in human cancers. Nat. Genet. **31:**295–300.
41. **Sap, J., Y.-P. Jiang, D. Friedlander, M. Grumet, and J. Schlessinger.** 1994. Receptor tyrosine phosphatase R-PTP-κ mediates homophilic binding. Mol. Cell. Biol. **14:**1–9.
42. **Schlaeger, T. M., Y. Qin, Y. Fujiwara, J. Magram, and T. N. Sato.** 1995. Vascular endothelial cell lineage-specific promoter in transgenic mice. Development **121:**1089–1098.
43. **Suzuki, E., D. Nagata, M. Yoshizumi, M. Kakoki, A. Goto, M. Omata, and Y. Hirata.** 2000. Reentry into the cell cycle of contact-inhibited vascular endothelial cells by a phosphatase inhibitor. Possible involvement of extracellular signal-regulated kinase and phosphatidylinositol 3-kinase. J. Biol. Chem. **275:**3637–3644.
44. **Takahashi, N., A. Haba, F. Matsuno, and B. K. Seon.** 2001. Antiangiogenic therapy of established tumors in human skin/severe combined immunodeficiency mouse chimeras by anti-endoglin (CD105) monoclonal antibodies, and synergy between anti-endoglin antibody and cyclophosphamide. Cancer Res. **61:**7846–7854.
45. **Takahashi, T., K. Takahashi, R. Mernaugh, V. Drozdoff, C. Sipe, H. Schoecklmann, B. Robert, D. R. Abrahamson, and T. O. Daniel.** 1999. Endothelial localization of receptor tyrosine phosphatase, ECRTP/DEP-1, in developing and mature renal vasculature. J. Am. Soc. Nephrol. **10:**2135–2145.
46. **Takahashi, Y., T. Imanaka, and T. Takano.** 1996. Spatial and temporal pattern of smooth muscle cell differentiation during development of the vascular system in the mouse embryo. Anat. Embryol. (Berlin) **194:**515–526.
47. **Trapasso, F., R. Iuliano, A. Boccia, A. Stella, R. Visconti, P. Bruni, G. Baldassarre, M. Santoro, G. Viglietto, and A. Fusco.** 2000. Rat protein tyrosine phosphatase η suppresses the neoplastic phenotype of retrovirally transformed thyroid cells through the stabilization of $p27^{Kip1}$. Mol. Cell. Biol. **20:**9236–9246.
48. **Van Vactor, D.** 1998. Protein tyrosine phosphatases in the developing nervous system. Curr. Opin. Cell Biol. **10:**174–181.
49. **Wang, H. U., Z. F. Chen, and D. J. Anderson.** 1998. Molecular distinction and angiogenic interaction between embryonic arteries and veins revealed by ephrin-B2 and its receptor Eph-B4. Cell **93:**741–753.
50. **Wartenberg, M., J. Gunther, J. Hescheler, and H. Sauer.** 1998. The embryoid body as a novel in vitro assay system for antiangiogenic agents. Lab. Investig. **78:**1301–1314.
51. **Xue, Y., X. Gao, C. E. Lindsell, C. R. Norton, B. Chang, C. Hicks, M. Gendron-Maguire, E. B. Rand, G. Weinmaster, and T. Gridley.** 1999. Embryonic lethality and vascular defects in mice lacking the Notch ligand Jagged1. Hum. Mol. Genet. **8:**723–730.
52. **Yagi, T., S. Nada, N. Watanabe, H. Tamemoto, N. Kohmura, Y. Ikawa, and S. Aizawa.** 1993. A novel negative selection for homologous recombinants using diphtheria toxin A fragment gene. Anal. Biochem. **214:**77–86.
53. **Zhang, L., M. L. Martelli, C. Battaglia, F. Trapasso, D. Tramontano, G. Viglietto, A. Porcellini, M. Santoro, and A. Fusco.** 1997. Thyroid cell transformation inhibits the expression of a novel rat protein tyrosine phosphatase. Exp. Cell Res. **235:**62–70.
54. **Zhao, G. Q., K. Deng, P. A. Labosky, L. Liaw, and B. L. Hogan.** 1996. The gene encoding bone morphogenetic protein 8B is required for the initiation and maintenance of spermatogenesis in the mouse. Genes Dev. **10:**1657–1669.